Exciton band structure in two-dimensional materials

Pierluigi Cudazzo, Lorenzo Sponza, Christine Giorgetti, Lucia Reining, Francesco Sottile, Matteo Gatti

Supplementary Material for Exciton band structure in two-dimensional materials

Pierluigi Cudazzo,[1,2] Lorenzo Sponza,[3] Christine Giorgetti,[1,2]
Lucia Reining,[1,2] Francesco Sottile,[1,2] and Matteo Gatti[1,2,4]

[1] *Laboratoire des Solides Irradiés, École Polytechnique, CNRS, CEA, Université Paris-Saclay, F-91128 Palaiseau, France*
[2] *European Theoretical Spectroscopy Facility (ETSF)*
[3] *Department of Physics, King's College London, London WC2R 2LS, United Kingdom*
[4] *Synchrotron SOLEIL, L'Orme des Merisiers, Saint-Aubin, BP 48, F-91192 Gif-sur-Yvette, France*

(Dated: November 25, 2015)

I. COMPUTATIONAL DETAILS FOR GRAPHANE AND h-BN

All calculations have been done in a plane-wave basis using a supercell approach. For graphane we have adopted the crystal structure optimized in Ref. 1. For the h-BN monolayer we have fixed the atoms in their experimental bulk positions. The single layers have been separated by 20 Å vacuum space in h-BN and 15 Å in graphane to prevent artificial interactions between periodic replicas. DFT calculations in the LDA, for which we have used standard Troullier-Martins pseudopotentials[2], are converged with a plane-wave cutoff of 40 Hartree for graphane and 50 Hartree for h-BN. We have used a Γ-centered 45×45×1 **k**-point grid for graphane and 48×48×1 for h-BN.

In GW calculations, in order to facilitate the convergence with the number of empty states (which becomes prohibitively expensive with the increase of vacuum space), we have adopted the effective-energy technique (EET)[3]. This allows obtaining converged results for both systems by using only 90 bands for the calculation of the screened Coulomb interaction W and 60 bands for self-energy corrections within the one-shot G_0W_0 framework[4]. The dielectric function ϵ in reciprocal space is converged with 11.5 and 15 Hartree cutoff for graphane and h-BN, respectively. In this way the G_0W_0 correction to the fundamental gap is 2.85 eV in graphane and 2.80 eV in h-BN. This yields a QP band gap of 6.22 eV and 7.36 eV, respectively.

In BSE calculations, to converge the spectra in the considered energy range, we have included five valence and five conduction bands for graphane, while for h-BN we used three valence and four conduction bands. To take into account crystal local-field effects[4], we have considered a dielectric function of size 589 **G** vectors for both systems.

For DFT and GW calculations we have used a modified version of Abinit[5]. For BSE calculations we have used the EXC code[6].

II. COULOMB INTERACTION

We have used the 2D Coulomb cutoff proposed in Ref. 7. For a single layer oriented perpendicular to the z axis, the effective Coulomb interaction in reciprocal space thus reads:

$$\tilde{v}_c(\mathbf{k}) = \frac{4\pi}{k^2}\left[1 + e^{-k_\parallel z_0}\left(\frac{k_z}{k_\parallel}\sin(k_z z_0) - \cos(k_z z_0)\right)\right] \tag{1}$$

with $k^2 = k_\parallel^2 + k_z^2$ (where $\mathbf{k} = \mathbf{q}+\mathbf{G}$ is the sum of a vector $\mathbf{q}$ belonging to the first Brillouin zone and a reciprocal-lattice vector $\mathbf{G}$). Setting the cutoff distance $z_0 = L_z/2$ (where L_z is the interlayer distance) and using 2D **k**-point grids, the $\sin(k_z z_0)$ term in Eq. (1) vanishes[7] in all $\mathbf{G}_z \neq 0$. Hence expression (1) is regular in every **k** point of the mesh, except in $\mathbf{k} = 0$, where it diverges as k^{-2}.

The truncated Coulomb interaction (1) is then used whenever sums over **G** are performed, as in the solution of the RPA Dyson equation $\chi = \chi_0 + \chi_0\tilde{v}_c\chi$, in the calculation of $W = \epsilon^{-1}\tilde{v}_c$ and of the matrix elements of the BSE kernel. On the contrary, spectra are calculated[8,9] with the untruncated Coulomb interaction v_c as: $\epsilon^{-1} = 1 + v_c\chi$ since in this case the Coulomb interaction enters as an external potential.

Matrix elements of $W = \epsilon^{-1}\tilde{v}_c$ are needed in both GW and BSE calculations that require Brillouin-zone summations including the $\mathbf{q} = \mathbf{G} = 0$ singular term of $\tilde{v}_c$ (1). Following Ref. 10, we remove the Coulomb singularity by an analytical integration of $\tilde{v}_c$ in a small volume Q_0 around $\mathbf{q} = 0$. The leading term of (1) for $\mathbf{G} = 0$ and in-plane $\mathbf{q} \to 0$ is:

$$\tilde{v}_c(\mathbf{q} \to 0) = \frac{4\pi z_0}{q^2} \tag{2}$$

By defining:

$$I_{sz} = \frac{N_k}{\Omega}\int_{Q_0} d\mathbf{q}\frac{4\pi z_0}{q^2}, \tag{3}$$

we obtain[9]:

$$I_{sz} = 4\pi\frac{6\log(3)}{12^{1/4}}\frac{Hz_0}{Q_0}\sqrt{A_0}, \tag{4}$$

where $Q_0 = \Omega/N_k = HA_0$, Ω is the volume of the first Brillouin zone, N_k is the number of **k** points, A_0 is the

hexagonal area laying on the xy plane and centered in $\mathbf{q} = 0$, H is height of Q_0. Additionally in Eq. (4) we have made use of the approximation $\int_{Q_0} \approx H \int_{A_0}$.

III. EXCITON ANALYSIS

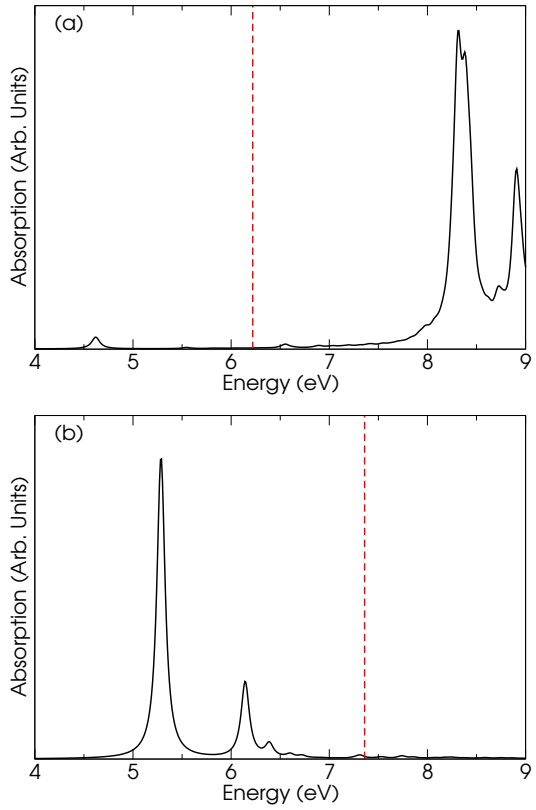

FIG. 1. Absorption spectrum of (a) graphane and (b) h-BN. The red dashed lines represent the position of the QP band gap in the two systems.

Figs. 1(a)-(b) display the absorption spectra $\mathrm{Im}\epsilon_M$ at vanishing momentum transfer along ΓM for graphane and h-BN respectively. The lowest excited state gives rise to a peak inside the QP gap that is located at 4.6 eV in graphane and 5.3 eV in h-BN. In both systems the onset of the spectrum is related to two degenerate bound excitons: only one is visible along this direction while the other one is dark. In the following, we will focus on the analysis of the bright excitons.

The wavefunction for the exciton λ expanded in the basis of independent valence-conduction (v-c) transitions for $\mathbf{q} = 0$ reads:

$$\Psi^{\lambda}_{\mathbf{q}=0}(\mathbf{r}_h, \mathbf{r}_e) = \sum_{vc\mathbf{k}} A^{\lambda}_{vc\mathbf{k}} \phi_{v\mathbf{k}}(\mathbf{r}_h) \phi_{c\mathbf{k}}(\mathbf{r}_e), \qquad (5)$$

where the sum is over the $\mathbf{k}$ points of the first Brillouin zone. The mixing coefficients $A^{\lambda}_{vc\mathbf{k}}$ are the eigenvectors that are obtained as the solution of the Bethe-Salpeter equation[4]. For both graphane and h-BN the two lowest-energy degenerate excitons are related to transitions between top-valence and bottom-conduction bands. Fig. 2 shows, for those bands, the modulus of the coefficients $|A^{\lambda}_{vc\mathbf{k}}|$ as a function of $\mathbf{k}$ for the bright excitons of the two systems. In the left panel of Fig. 2 we see that for hBN the largest weights are found around the K point and along the KM line of the hexagonal first Brillouin zone. In this part of Brillouin zone both valence and conduction bands are flat (see the upper panel of Fig. 3). For graphane (see the right panel of Fig. 2), on the other hand, $|A^{\lambda}_{vc\mathbf{k}}|$ is larger for $\mathbf{k}$ around the Γ point, where both valence and conduction bands are parabolic (see the bottom panel of Fig. 3). This suggests that in

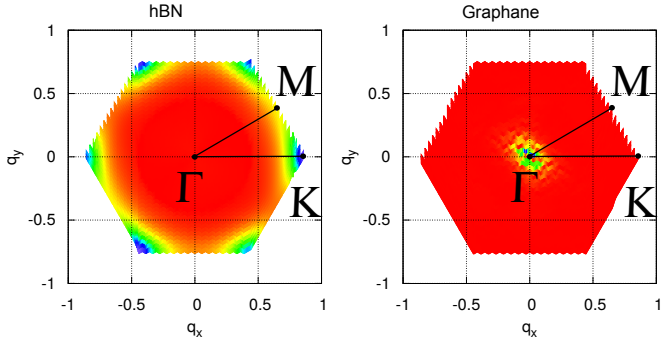

FIG. 2. Excitonic eigenvectors $|A^{\lambda}_{vc\mathbf{k}}|$ for the top-valence v and bottom conduction c bands as a function of $\mathbf{k}$ for the bright exciton of h-BN (on the left side) and graphane (on the right side).

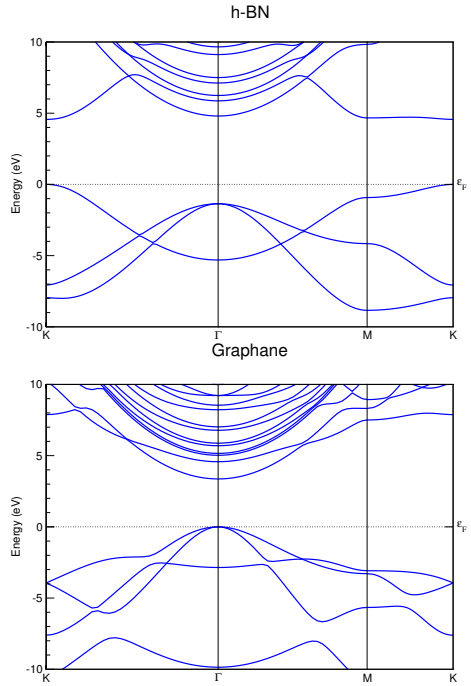

FIG. 3. LDA band structures of hBN (upper panel) and graphane (bottom panel).

h-BN the exciton is Frenkel-like, while in graphane it is Wannier-like. We found a similar behaviour for the other degenerate dark excitons at $\mathbf{q} = 0$.

IV. EXCITONIC HAMILTONIAN IN A BASIS OF LOCALIZED WAVEFUNCTIONS

In the following we consider a two-band system and write the corresponding BSE excitonic Hamiltonian[4] in a basis of electronic wavefunctions localized on lattice sites[11–13]:

$$\hat{H}_{ex} = \sum_{\mathbf{R},\mathbf{S}} h^c_{\mathbf{R},\mathbf{S}} a^\dagger_{\mathbf{R}} a_{\mathbf{S}} - \sum_{\mathbf{R},\mathbf{S}} h^v_{\mathbf{R},\mathbf{S}} b^\dagger_{\mathbf{R}} b_{\mathbf{S}} + \sum_{\mathbf{R},\mathbf{S},\mathbf{P},\mathbf{Q}} (v^{\mathbf{S},\mathbf{P}}_{\mathbf{Q},\mathbf{R}} - W^{\mathbf{S},\mathbf{P}}_{\mathbf{Q},\mathbf{R}}) a^\dagger_{\mathbf{R}} b^\dagger_{\mathbf{Q}} b_{\mathbf{S}} a_{\mathbf{P}}, \tag{6}$$

with:

$$v^{\mathbf{S},\mathbf{P}}_{\mathbf{Q},\mathbf{R}} = \int d\mathbf{r} \int d\mathbf{r}' \psi^*_c(\mathbf{r}-\mathbf{R}) \psi^*_v(\mathbf{r}'-\mathbf{S}) v_c(\mathbf{r},\mathbf{r}') \psi_v(\mathbf{r}-\mathbf{Q}) \psi_c(\mathbf{r}'-\mathbf{P}) \tag{7}$$

$$W^{\mathbf{S},\mathbf{P}}_{\mathbf{Q},\mathbf{R}} = \int d\mathbf{r} \int d\mathbf{r}' \psi^*_c(\mathbf{r}-\mathbf{R}) \psi^*_v(\mathbf{r}'-\mathbf{S}) W(\mathbf{r},\mathbf{r}') \psi_c(\mathbf{r}-\mathbf{P}) \psi_v(\mathbf{r}'-\mathbf{Q}). \tag{8}$$

Here the boldface letters indicate the lattice vectors, $a^\dagger$ (a) and $b^\dagger$ (b) are creation (annihilation) operators for electrons and holes, respectively; h^c is the single-particle hamiltonian describing the motion of independent electrons: $h^c_{\mathbf{R}i,\mathbf{S}j} = E^c \delta_{\mathbf{R}i,\mathbf{S}j} + t^c_{\mathbf{R}i,\mathbf{S}j}$, where E^c is the electron level and t^c is the electron hopping integral, which gives rise to the dispersion of the electronic band in the periodic crystal (h^v, E^v and t^v are defined correspondingly for holes). Suppressing the hopping terms is equivalent to considering bands without dispersion, i.e. completely flat. In the integrals in Eqs. (7)-(8), the bare Coulomb interaction v_c and the statically screened Coulomb interaction W act as an exchange and a direct electron-hole interaction, respectively[14]. The former is absent for triplet excitations[15].

In this representation the excitonic wavefunction can be written as a superposition of electron-hole pairs localized on different sites:

$$|\Psi_{ex}\rangle = \sum_{\mathbf{R}} e^{i\mathbf{q}\cdot\mathbf{R}} \sum_{\mathbf{S}} C^{\mathbf{q}}_{\mathbf{S}} a^\dagger_{\mathbf{R}} b^\dagger_{\mathbf{R}+\mathbf{S}} |0\rangle, \tag{9}$$

where the coefficient $C^{\mathbf{q}}_{\mathbf{S}}$ are given by solution of the secular problem:

$$\sum_{\mathbf{S}'} \left[h^c_{\mathbf{R},\mathbf{R}+\mathbf{S}-\mathbf{S}'} e^{i\mathbf{q}\cdot(\mathbf{S}-\mathbf{S}')} - h^v_{\mathbf{R}+\mathbf{S},\mathbf{R}+\mathbf{S}'} + \sum_{\mathbf{R}'} \left(v^{\mathbf{R}'+\mathbf{S}',\mathbf{R}'}_{\mathbf{R}+\mathbf{S},\mathbf{R}} - W^{\mathbf{R}'+\mathbf{S}',\mathbf{R}'}_{\mathbf{R}+\mathbf{S},\mathbf{R}} \right) e^{i\mathbf{q}\cdot(\mathbf{R}'-\mathbf{R})} \right] C^{\mathbf{q}}_{\mathbf{S}'} = E_{ex}(\mathbf{q}) C^{\mathbf{q}}_{\mathbf{S}}. \tag{10}$$

To better understand the role played by the different terms in the excitonic hamiltonian we rewrite Eq. (6) in the following form:

$$\begin{aligned}
\hat{H}_{ex} = &\sum_{\mathbf{R}} E_c a^\dagger_{\mathbf{R}} a_{\mathbf{R}} - \sum_{\mathbf{R}} E_v b^\dagger_{\mathbf{R}} b_{\mathbf{R}} + \sum_{\mathbf{R},\mathbf{S}} (v^{\mathbf{S},\mathbf{S}}_{\mathbf{R},\mathbf{R}} - W^{\mathbf{S},\mathbf{S}}_{\mathbf{R},\mathbf{R}}) a^\dagger_{\mathbf{R}} b^\dagger_{\mathbf{R}} b_{\mathbf{S}} a_{\mathbf{S}} - \sum_{\mathbf{R},\mathbf{S}} (1-\delta_{\mathbf{S},\mathbf{R}}) W^{\mathbf{S},\mathbf{R}}_{\mathbf{S},\mathbf{R}} a^\dagger_{\mathbf{R}} b^\dagger_{\mathbf{S}} b_{\mathbf{S}} a_{\mathbf{R}} + \\
&\sum_{\mathbf{R},\mathbf{S}} t^c_{\mathbf{R},\mathbf{S}} a^\dagger_{\mathbf{R}} a_{\mathbf{S}} - \sum_{\mathbf{R},\mathbf{S}} t^v_{\mathbf{R},\mathbf{S}} b^\dagger_{\mathbf{R}} b_{\mathbf{S}} + \sum_{\mathbf{R},\mathbf{S},\mathbf{P},\mathbf{Q}} (1-\delta_{\mathbf{R},\mathbf{P}})(1-\delta_{\mathbf{Q},\mathbf{S}})(1-\delta_{\mathbf{Q},\mathbf{R}})(1-\delta_{\mathbf{P},\mathbf{S}}) (v^{\mathbf{S},\mathbf{P}}_{\mathbf{Q},\mathbf{R}} - W^{\mathbf{S},\mathbf{P}}_{\mathbf{Q},\mathbf{R}}) a^\dagger_{\mathbf{R}} b^\dagger_{\mathbf{Q}} b_{\mathbf{S}} a_{\mathbf{P}} + \\
&\sum_{\mathbf{R},\mathbf{S},\mathbf{P}} (1-\delta_{\mathbf{P},\mathbf{S}}) (v^{\mathbf{S},\mathbf{P}}_{\mathbf{R},\mathbf{R}} - W^{\mathbf{S},\mathbf{P}}_{\mathbf{R},\mathbf{R}}) a^\dagger_{\mathbf{R}} b^\dagger_{\mathbf{R}} b_{\mathbf{S}} a_{\mathbf{P}} + \sum_{\mathbf{R},\mathbf{S},\mathbf{Q}} (1-\delta_{\mathbf{R},\mathbf{Q}}) (v^{\mathbf{S},\mathbf{S}}_{\mathbf{R},\mathbf{Q}} - W^{\mathbf{S},\mathbf{S}}_{\mathbf{R},\mathbf{Q}}) a^\dagger_{\mathbf{R}} b^\dagger_{\mathbf{Q}} b_{\mathbf{S}} a_{\mathbf{S}} + \sum_{\mathbf{R},\mathbf{S}} (1-\delta_{\mathbf{S},\mathbf{R}}) v^{\mathbf{S},\mathbf{R}}_{\mathbf{S},\mathbf{R}} a^\dagger_{\mathbf{R}} b^\dagger_{\mathbf{S}} b_{\mathbf{S}} a_{\mathbf{R}}.
\end{aligned} \tag{11}$$

The first four terms (i.e. the first line) can be interpreted as the sum of a Frenkel (FR) and a charge-transfer (CT) hamiltonian describing respectively pure Frenkel excitons (with the electron and the hole localised on the same lattice site) and delocalised charge-transfer excitons (with the electron and the hole localised on different lattices sites). The fifth and sixth terms, related to the hopping t^v and t^c, contribute to FR-CT and CT-CT coupling. The other remaining terms involving overlap integrals between electronic wavefunctions localized on different sites also contribute to CT-CT and FR-CT coupling. If the overlap between the electronic wavefunctions localized on

different sites is small, these terms are in general smaller than the hopping terms. Thus, in the following we will neglect them. This approximation does not introduce a loss of generality since in Eq. (11) hopping and overlap integrals, having similar mathematical expression, play the same role: they couple excitons of different nature. As a consequence, the small overlap contribution would only renormalize the hopping without introducing new effects. Therefore, in the following we limit the discussion to the effect of the hopping.

Neglecting also the hopping terms t^v and t^c, the excitonic hamiltonian (11) factorizes in a FR and a CT hamiltonian [only the first line of Eq. (11) is left] so that the neutral excitations of the systems are pure FR and pure CT excitons (localised on the site $\mathbf{R}_i \neq 0$):

$$|\Psi_{FR}\rangle = \sum_{\mathbf{R}} e^{i\mathbf{q}\cdot\mathbf{R}} a^\dagger_{\mathbf{R}} b^\dagger_{\mathbf{R}} |0\rangle \tag{12}$$

$$|\Psi^{(i)}_{CT}\rangle = \sum_{\mathbf{R}} e^{i\mathbf{q}\cdot\mathbf{R}} a^\dagger_{\mathbf{R}} b^\dagger_{\mathbf{R}+\mathbf{R}_i} |0\rangle. \tag{13}$$

We note that for both FR and CT states the square modulus of the excitonic wavefunction for fixed position of the hole (i.e. for fixed $\mathbf{R}$ in this representation) is independent of the wavevector $\mathbf{q}$. The corresponding energy levels are given by the following equations:

$$E_{FR}(\mathbf{q}) = E_c - E_v - \mathcal{W} + \mathcal{I}(\mathbf{q}) - \mathcal{W}'(\mathbf{q}) \tag{14}$$

$$E^{(i)}_{CT} = E_c - E_v - \tilde{\mathcal{W}}_i, \tag{15}$$

where we have introduced the excitation transfer interaction[16] due to the exchange e-h interaction:

$$\mathcal{I}(\mathbf{q}) = \sum_{\mathbf{R}'} v^{\mathbf{R}',\mathbf{R}'}_{\mathbf{R},\mathbf{R}} e^{i\mathbf{q}(\mathbf{R}'-\mathbf{R})}, \tag{16}$$

the on-site direct e-h interaction $\mathcal{W} = W^{\mathbf{R},\mathbf{R}}_{\mathbf{R},\mathbf{R}}$, and the off-site direct e-h interaction $\tilde{\mathcal{W}}_i = W^{\mathbf{R}+\mathbf{R}_i,\mathbf{R}}_{\mathbf{R}+\mathbf{R}_i,\mathbf{R}}$. They derive from the third and fourth term in Eq. (11) respectively. In addition, the term

$$\mathcal{W}'(\mathbf{q}) = \sum_{\mathbf{R}'\neq\mathbf{R}} W^{\mathbf{R}',\mathbf{R}'}_{\mathbf{R},\mathbf{R}} e^{i\mathbf{q}(\mathbf{R}'-\mathbf{R})} \tag{17}$$

derives from the third term in the first line of Eq. (11) as well. $\mathcal{W}'$ involves overlap integrals between electronic wavefunctions on different sites and, similarly to $\mathcal{I}$, induces scattering processes of an e-h pair from one site to another. We emphasize that, in contrast to the other terms involving overlap integrals in Eq. (11) [not considered in Eq. (14)], $\mathcal{W}'$ always couples e-h pairs with the electron and the hole located on the same site. Hence, in principle there is no reason to neglect it. However, contrarily to the exchange e-h interaction $\mathcal{I}$, this term involves overlap integrals so that it is a short-range interaction. Thus, the sum in Eq. (17) can be restricted to the first nearest neighbours. Moreover, the exponential in Eq. (17) is actually a sum of cosine functions only, as the corresponding antisymmetric sine function terms sum to zero. So $\mathcal{W}'(\mathbf{q})$ at small $\mathbf{q}$ is just a constant term independent of $\mathbf{q}$ plus a quadratic term in $\mathbf{q}$: $\mathcal{W}'(\mathbf{q}) \sim A + Bq^2 + o(q^4)$.

This analysis implies that the effect of the direct interaction on the exciton dispersion at small $\mathbf{q}$ is negligible with respect to the exchange e-h interaction which is linear (see sectionV). We can conclude that the term $\mathcal{W}'(\mathbf{q})$ in Eq. (14) can be neglected. Therefore, from Eqs. (14)-(15) we find that pure CT excitons do not disperse as a function of $\mathbf{q}$, while for a FR exciton the dispersion is set by the exchange e-h interaction through $\mathcal{I}$. In the triplet channel, for which there is no exchange e-h interaction in the hamiltonian, the dispersion is zero for both FR and CT excitons.

So far we have neglected the hopping terms. In this picture, the effect of the hopping can be treated as a perturbation. Here we focus on its effect on the lowest excited state that we assume to be a FR exciton. At first order in the perturbation, the exciton wavefunction is given by:

$$|\psi^\lambda_{\mathbf{q}}\rangle = |\psi^\lambda_{FR}\rangle + \sum_i C^\lambda_i(\mathbf{q}) |\psi^{(i)}_{CT}\rangle, \tag{18}$$

where $|\psi_{FR}\rangle$ and $|\psi^{(i)}_{CT}\rangle$ are pure FR and CT states that depend on $\mathbf{q}$ only through a phase factor. The larger the mixing coefficients $C^\lambda_i(\mathbf{q})$, the more delocalised the Frenkel exciton becomes.

In perturbation theory, the mixing coefficients $C_i(\mathbf{q})$ can be expressed in terms of the hopping integrals of the valence and conduction bands t^v and t^c, the energy of the FR exciton E_{FR}, the energy of the CT exciton E^i_{CT}, and the lattice vector $\mathbf{R}_i$ that define the CT state:

$$C^\lambda_i(\mathbf{q}) = \frac{t^c_{\mathbf{R},\mathbf{R}+\mathbf{R}i} e^{i\mathbf{q}\cdot\mathbf{R}_i} - t^v_{\mathbf{R},\mathbf{R}+\mathbf{R}i}}{E_{FR}(\mathbf{q}) - E^i_{CT}}. \tag{19}$$

These mixing coefficients are hence strongly dependent on the wavevector $\mathbf{q}$. As a consequence, the exciton wavefunction $|\psi^\lambda_{\mathbf{q}}\rangle$ changes its shape as a function of $\mathbf{q}$ due to the coupling between FR and CT states. In particular, we can identify two effects.

The first one is related to the $\mathbf{q}$ dependence of the FR state energy through the exchange e-h interaction. As $q = |\mathbf{q}|$ increases, the linear behavior of $\mathcal{I}(\mathbf{q})$ increases the energy $E_{FR}(\mathbf{q})$ of the FR exciton (see sectionV), which becomes closer to the energies E^i_{CT} of CT states (that are independent of $\mathbf{q}$). Since the differences $E_{FR}(\mathbf{q}) - E^i_{CT}$ become smaller at the denominator of Eq. (19), this enhances the coupling between the two excitations. This causes an isotropic delocalization of the wavefunction of the Frenkel exciton, since the coupling with the CT excitons identified by different $\mathbf{R}_i$ changes in the same manner.

The second effect is related to the explicit $\mathbf{q}$-dependence of the hopping term at the numerator of Eq. (19), where the scalar product $\mathbf{q}\cdot\mathbf{R}_i$ appears in the exponential. As $q = |\mathbf{q}|$ increases, the scalar product is always

zero for $\mathbf{R}_i$ perpendicular to $\mathbf{q}$, hence the exponential is always 1, while for all the other $\mathbf{R}_i$ the exponential changes. This induces a different coupling with the CT excitons identified by different $\mathbf{R}_i$, causing an anisotropic variation of the wavefunction of the Frenkel exciton as a function of $\mathbf{q}$.

Finally, the first non-trivial term in the perturbative expansion of the exciton energy is the second-order one:

$$\Delta E(\mathbf{q}) = \sum_i \frac{|t^c_{\mathbf{R},\mathbf{R}+\mathbf{R}i}|^2 + |t^v_{\mathbf{R},\mathbf{R}+\mathbf{R}i}|^2}{|E_{FR}(\mathbf{q}) - E^i_{CT}|^2} - \sum_i \frac{t^c_{\mathbf{R},\mathbf{R}+\mathbf{R}i} t^v_{\mathbf{R},\mathbf{R}+\mathbf{R}i} \cos(\mathbf{q}\cdot\mathbf{R}_i)}{|E_{FR}(\mathbf{q}) - E^i_{CT}|^2}, \quad (20)$$

which at small $\mathbf{q}$ is quadratic in $\mathbf{q}$ for the cosine function in the numerator of the second term. As a consequence, in the optical limit, the effect of this term on the exciton dispersion is negligible with respect to the exchange e-h interaction $\mathcal{I}(\mathbf{q})$ which is linear in $\mathbf{q}$. On the other hand it becomes important at large $\mathbf{q}$ when the exchange e-h interaction is constant (see sectionV).

V. EXCHANGE ELECTRON-HOLE INTERACTION

Assuming that the electronic wavefunctions can be factorized in an in-plane $\phi(\boldsymbol{\rho})$ and out-of-plane $\chi(z)$ components so that $\psi(\mathbf{r}) = \phi(\boldsymbol{\rho})\chi(z)$ and writing the Coulomb potential v_c in terms of its 2D partial Fourier transform:

$$\frac{1}{|\mathbf{r}-\mathbf{r}'|} = \sum_{\mathbf{q}'\mathbf{G}} \frac{2\pi}{|\mathbf{q}'+\mathbf{G}|} e^{i(\mathbf{q}'+\mathbf{G})\cdot(\boldsymbol{\rho}-\boldsymbol{\rho}')} e^{-|\mathbf{q}'+\mathbf{G}|(z-z')}, \quad (21)$$

the matrix elements (7) of the Coulomb potential become:

$$\begin{aligned} v^{\mathbf{R}'\mathbf{R}'}_{\mathbf{R}\mathbf{R}} &= \sum_{\mathbf{q}'\mathbf{G}} \frac{2\pi\beta(\mathbf{q}'+\mathbf{G})}{|\mathbf{q}'+\mathbf{G}|} \int d\boldsymbol{\rho} \int d\boldsymbol{\rho}' \phi^*_c(\boldsymbol{\rho}-\mathbf{R})\phi^*_v(\boldsymbol{\rho}'-\mathbf{R}') e^{i(\mathbf{q}'+\mathbf{G})\cdot(\boldsymbol{\rho}-\boldsymbol{\rho}')} \phi_v(\boldsymbol{\rho}-\mathbf{R})\phi_c(\boldsymbol{\rho}'-\mathbf{R}') \\ &= \sum_{\mathbf{q}'\mathbf{G}} \frac{2\pi\beta(\mathbf{q}'+\mathbf{G})}{|\mathbf{q}'+\mathbf{G}|} \int d\boldsymbol{\rho} \phi^*_c(\boldsymbol{\rho}) e^{i(\mathbf{q}'+\mathbf{G})\cdot\boldsymbol{\rho}} \phi_v(\boldsymbol{\rho}) \int d\boldsymbol{\rho}' \phi^*_v(\boldsymbol{\rho}') e^{-i(\mathbf{q}'+\mathbf{G})\cdot\boldsymbol{\rho}'} \phi_c(\boldsymbol{\rho}') e^{i(\mathbf{q}'+\mathbf{G})\cdot(\mathbf{R}-\mathbf{R}')} \end{aligned} \quad (22)$$

where:

$$\beta(\mathbf{q}'+\mathbf{G}) = \int dz \int dz' \chi^*_c(z)\chi^*_v(z') e^{-|\mathbf{q}'+\mathbf{G}|(z-z')} \chi_v(z)\chi_c(z'). \quad (23)$$

Inserting Eq. (22) into Eq. (16) we obtain the following expression:

$$\mathcal{I}(\mathbf{q}) = \sum_{\mathbf{G}} \frac{2\pi\beta(\mathbf{q}+\mathbf{G})}{|\mathbf{q}+\mathbf{G}|} \langle c|e^{i(\mathbf{q}+\mathbf{G})\cdot\boldsymbol{\rho}}|v\rangle\langle v|e^{-i(\mathbf{q}+\mathbf{G})\cdot\boldsymbol{\rho}}|c\rangle. \quad (24)$$

For small momentum transfer inside the first Brillouin zone the dominant term in Eq. (24) is $\mathbf{G} = 0$. Thus we neglect the terms $\mathbf{G} \neq 0$, which is equivalent to neglect the in-plane crystal local fields[4]. Moreover we take the dipole approximation for the matrix elements in Eq. (24). Under these conditions the expression for the excitation transfer interaction becomes:

$$\mathcal{I}(\mathbf{q}) = 2\pi q\beta(q)(\hat{\mathbf{q}}\cdot\boldsymbol{\mu}_{cv})(\hat{\mathbf{q}}\cdot\boldsymbol{\mu}_{vc}) \quad (25)$$

where $\hat{\mathbf{q}}$ is the unitary vector which defines the direction of the momentum transfer,

$$\boldsymbol{\mu}_{cv} = \int d\boldsymbol{\rho} \phi^*_c(\boldsymbol{\rho})\boldsymbol{\rho}\phi_v(\boldsymbol{\rho}) \quad (26)$$

is the dipole matrix element and $q = |\mathbf{q}|$. Finally, if we take for $\chi(z)$ the simplest form (i.e. constant inside the 2D slab and zero elsewhere): $\chi(z) = 1/\sqrt{d}$ for $|z| < d/2$ and $\chi(z) = 0$ for $|z| > d/2$ we obtain the following expression for $\beta(q)$:

$$\beta(q) = \frac{2}{qd}\left[1 - \frac{1}{qd}(1 - e^{-qd})\right] \quad (27)$$

and $\mathcal{I}$ becomes:

$$\mathcal{I}(\mathbf{q}) = \frac{4\pi}{d}(\hat{\mathbf{q}}\cdot\boldsymbol{\mu}_{cv})(\hat{\mathbf{q}}\cdot\boldsymbol{\mu}_{vc})\left[1 - \frac{1}{qd}(1 - e^{-qd})\right] \quad (28)$$

which has a linear behaviour for $q \ll 1/d$ and reaches a constant value for $q \gg 1/d$ (see Fig. 4).

We emphasize that this result is general since the asymptotic behaviour of $\mathcal{I}$ is independent of the detailed structure of $\chi(z)$. At small momentum transfer the slab behaves as a 2D lattice of zero thickness ($\chi(z)$ is a Dirac delta centered at zero). This means that the exchange e-h interaction can be obtained using in Eq. (22) the 2D Coulomb potential that is responsible for the linear behaviour in the optical limit. In the opposite limit when q is very large respect to $1/d$ the electronic density normal to the plane is seen as a uniform distribution.

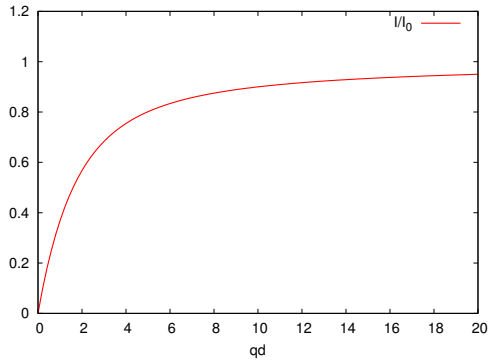

FIG. 4. The function $\mathcal{I}(\mathbf{q})/I_0$ where $I_0 = 4\pi/d\ (\hat{\mathbf{q}}\cdot\boldsymbol{\mu}_{cv})(\hat{\mathbf{q}}\cdot\boldsymbol{\mu}_{vc})$.

A more realistic expression for $\mathcal{I}$ can be obtained taking an exponential decay for $\chi(z)$: $\chi(z) = \frac{1}{\sqrt{\lambda}}e^{-|z|/\lambda}$. In this case we obtain the following expressions for β and $\mathcal{I}$:

$$\beta(q) = \frac{4+q\lambda}{(2+q\lambda)^2} \tag{29}$$

$$\mathcal{I}(\mathbf{q}) = 2\pi(\hat{\mathbf{q}}\cdot\boldsymbol{\mu}_{cv})(\hat{\mathbf{q}}\cdot\boldsymbol{\mu}_{vc})q\frac{4+q\lambda}{(2+q\lambda)^2} \tag{30}$$

which, taking $\lambda = d/2$, have the same asymptotic behaviour as Eq. (27) and Eq. (28).

VI. EXCITON DISPERSION IN h-BN AND GRAPHANE

The lowest-energy peak in the spectrum of both graphane and h-BN for $\mathbf{q} \to 0$ is related to two degenerate bound excitons in the singlet channel. In particular along the ΓM direction only one is visible and the other one is dark. At finite $\mathbf{q}$ the exciton degeneracy is removed. However, one exciton remains dark also at $\mathbf{q} \neq 0$.

By definition a dark exciton is not visible in the measured spectra. However, by diagonalising the excitonic hamiltonian $H_{\rm exc}\Psi^{\lambda}_{\mathbf{q}} = E^{\lambda}_{\mathbf{q}}\Psi^{\lambda}_{\mathbf{q}}$, it is possible to obtain the corresponding exciton eigenvalue $E^{\lambda}_{\mathbf{q}}$ and investigate its dispersion as a function of $\mathbf{q}$.

In Fig. 5 we show the dispersion for the dark and bright excitons of graphane which can be modeled as Wannier excitons. In the Wannier model[16–18], the exciton energies $E_\lambda(\mathbf{q})$ are:

$$E_\lambda(\mathbf{q}) = E_\lambda(\mathbf{q}=0) + \frac{q^2}{2(m_e+m_h)}, \tag{31}$$

where $E_\lambda(\mathbf{q}=0)$ is the exciton energy at $\mathbf{q}=0$, and m_e and m_h are the effective masses of the electron and the hole, respectively. The center of mass of the Wannier exciton behaves a free particle with a parabolic dispersion and an effective mass that is $m_e + m_h$.

By a parabolic fit of the dispersion we have obtained the effective mass of the two excitons in graphane, which

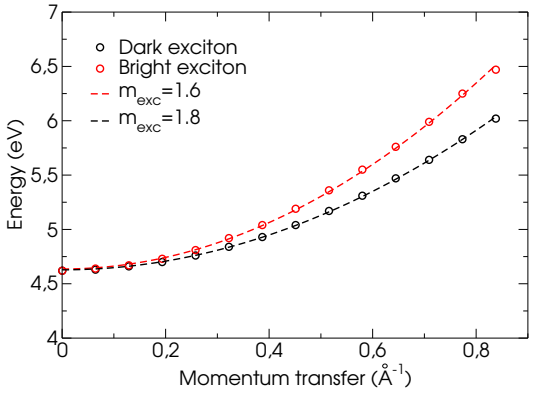

FIG. 5. Dark and bright exciton dispersion along the ΓM line in graphane in a two-band model. The dashed lines represent the parabolic fit.

is 1.6 and 1.8 for the bright and dark states, respectively. For the case of degenerate Wannier excitons, as in graphane, a direct link between the exciton mass and the electronic band structure is in principle more complicated than in Eq. (31)[19,20]. However, in the present case, since the two excitons have similar masses, we can directly compare the average value 1.7 of the effective mass with the sum $m_e + m_h = 1.3$ of the effective electron mass m_e and the average value m_h of the effective masses of the heavy and light holes at the Γ point in the electronic band structure. The two values match well confirming the Wannier character of the lowest excited states of graphane.

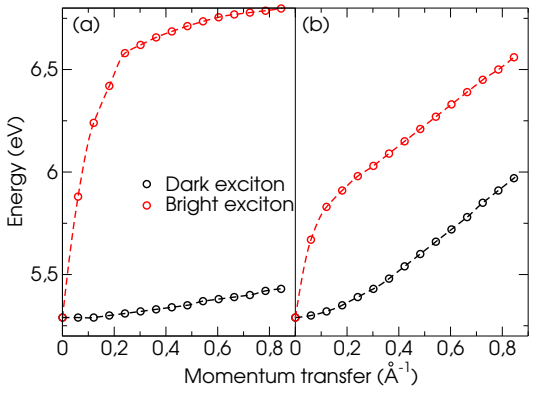

FIG. 6. (a) Dark and bright exciton dispersion along the ΓM line in h-BN in a two-band model with flat bands and (b) with the real electronic band structure.

We now consider the case of h-BN. On the basis of our model discussed in the previous section, the long-range part of the exchange e-h interaction $\mathcal{I}$ is proportional to the dipole matrix elements $\boldsymbol{\mu}_{vc}$ between valence and conduction states. As a consequence, the dark exciton of h-BN, for which $\boldsymbol{\mu}_{vc} = 0$, does not feel the long-range part of exchange e-h interaction [see Eq. (25)]. Thus, when the hopping is neglected, we expect that the dark exciton does not disperse as a function of $\mathbf{q}$. This is

confirmed by the solution of the BSE with flat bands. Indeed, Fig. 6(a) shows that, while the bright exciton has a linear dispersion at small $\mathbf{q}$ and then reaches a constant value, the energy of the dark state is almost constant. This also means that the short-range part of the exchange e-h interaction [the terms with $\mathbf{G} \neq 0$ in Eq. (24)], which has been neglected in the evaluation of $\mathcal{I}$ and that in principle is felt by both dark and bright excitons, does not have remarkable effects on the exciton dispersion. Finally, the hopping term [see Fig. 6(b)] modifies the dispersion of the bright exciton and induces a dispersion for the dark exciton. In practice, we see that, due to the lack of the long-range part of the exchange e-h interaction [see Eq. (25)], the dark exciton behaves like a triplet state.

VII. PHOSPHORENE

In Fig. 2 of the main article we have compared the exciton wavefunctions of the single layer of h-BN and graphane, which are representative cases for localised and delocalized excitons, respectively. BSE calculations in the literature have shown that also other classes of 2D semiconductors like transition-metal dichalcogenides (such as the monolayers of MoS_2[21,22], $MoSe_2$[23], WS_2[24]), phosphorene[25,26] (i.e. the single layer of black phosphorus), and hydrogenated or fluorinated group-IV 2D sheets (such as silicane,[27] germanane[27] or fluorographene[28], fluorosilicene,[29] etc.) in the optical limit display bound excitons whose wavefunctions for $\mathbf{q} \to 0$ are spread over several unit cells.

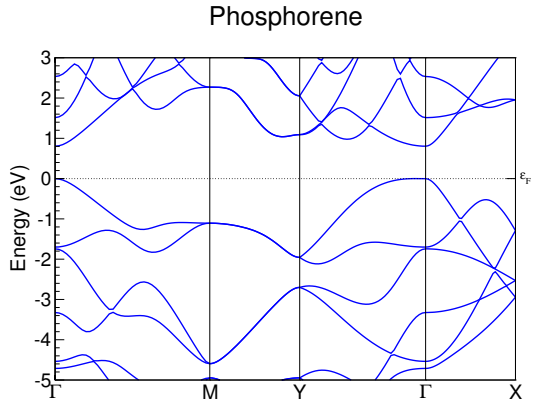

FIG. 7. LDA band structure of phosphorene.

In order to stress the materials-independent features of our studies, we show phosphorene as an additional example. Here we provide more details about our phosphorene calculations (the dispersion of the lowest exciton is shown in Fig. 3 of the main article). We have calculated the crystal structure of phosphorene (see Fig. 8) in the GGA (each layer was separated by 25 Å vacuum space). The lattice parameters (3.30 and 4.62 Å) that we have found are in very good agreement with those reported in the recent literature[30–32]. In the GW calculations[5], we have used a Γ-centered 44×44×1 $\mathbf{k}$-point grid, 60 bands with the EET method[3], and a 6 Hartree cutoff for the dielectric function. The G_0W_0 correction to the fundamental gap of the LDA band structure (see Fig. 7) is 1.4 eV, amounting to a direct QP gap at the Γ point of 2.2 eV (which is in excellent agreement with experiment[25]). In the BSE calculations[6], we have included two valence and four conduction bands.

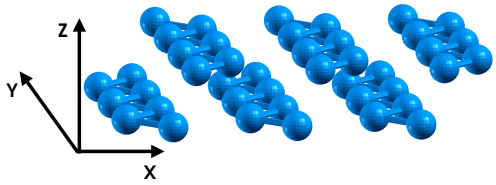

FIG. 8. Anisotropic crystal structure of phosphorene.

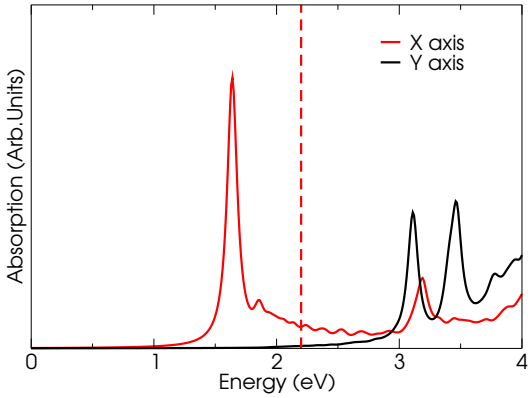

FIG. 9. Absorption spectum of phosphorene. The red dashed line marks the QP gap.

In Fig. 9 we show the absorption spectra at $\mathbf{q} \to 0$ momentum transfer evaluated along the X and Y directions. The anisotropic structure of phosphorene (see Fig. 8) is reflected in its optical properties. In the X direction the onset of the optical spectrum (peak at 1.64 eV) is set by the lowest-energy exciton involving top-valence and bottom-conduction bands, while along Y all the bound excitons inside the QP gap are dipole forbidden. The anisotropy is also responsible for the different dispersion of the lowest excited state along the ΓX and ΓY lines (see Fig. 10). In particular, as expected for a Wannier exciton, the dispersion is parabolic in both directions even though it is characterized by a different effective mass. This is related to the different dispersion of the valence and conduction bands along ΓX and ΓY (see Fig. 7) and demonstrates that in this system, like in graphane, the exciton behaviour as a function of the momentum transfer is set by the band structure also at small $\mathbf{q}$. Only

the optical limit along the two directions is qualitatively different. Along ΓY, due to the lack of the exchange e-h interaction [for a dark exciton $\boldsymbol{\mu}_{vc} = 0$: see Eq. (25)], the parabolic behaviour is preserved, hence $\nabla_{\mathbf{q}} E^{\lambda}_{\mathbf{q}} = 0$ for $\mathbf{q} \to 0$. Instead, along ΓX $\nabla_{\mathbf{q}} E^{\lambda}_{\mathbf{q}} \neq 0$ for $\mathbf{q} \to 0$: the exchange e-h interaction induces a linear dispersion as in the case of h-BN. However, due to the delocalization of the electronic wavefunction, the contribution coming from the exchange e-h interaction is so small with respect to the hopping, that its effect is visible only close to the optical limit.

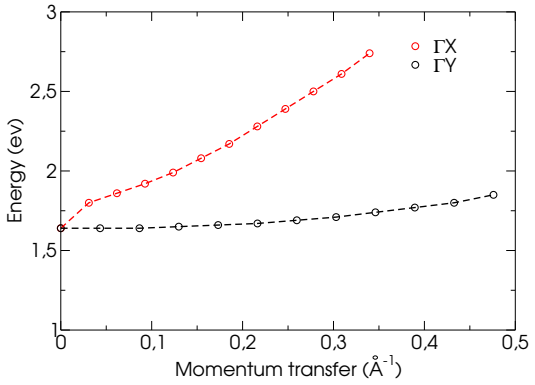

FIG. 10. Exciton dispersion along the ΓX and ΓY lines in phosphorene.

In conclusion, we have presented a general picture of the exciton dispersion as a function of its wavevector $\mathbf{q}$ for 2D semiconductors that consistently explains the results of the BSE calculations for h-BN, graphane and phosphorene. At small $\mathbf{q}$ the dispersion is set by the exchange e-h interaction and it is linear, while at large $\mathbf{q}$ it is set by the electronic band structure. The crossover between the two regimes is determined by the relative strengths of the exchange e-h interaction related to the dipole matrix element $\boldsymbol{\mu}_{vc}$, the hopping parameter and the effective thickness of the system. When the electronic wavefunctions are strongly delocalized, the contribution coming from the exchange e-h interaction becomes negligible and the hopping term dominates the dispersion (except for very small $\mathbf{q}$), as predicted by the Wannier model.

[1] P. Cudazzo, C. Attaccalite, I. V. Tokatly, and A. Rubio, Phys. Rev. Lett. **104**, 226804 (2010).
[2] N. Troullier and J. L. Martins, Phys. Rev. B **43**, 1993 (1991).
[3] J. A. Berger, L. Reining, and F. Sottile, Phys. Rev. B **82**, 041103 (2010).
[4] G. Onida, L. Reining, and A. Rubio, Rev. Mod. Phys. **74**, 601 (2002).
[5] X. Gonze, G. Rignanese, M. Verstraete, J. Beuken, Y. Pouillon, R. Caracas, F. Jollet, M. Torrent, G. Zerah, M. Mikami, P. Ghosez, M. Veithen, J. Raty, V. Olevano, F. Bruneval, L. Reining, R. Godby, G. Onida, D. Hamann, and D. Allan, Z. Kristallogr. **220**, 558 (2005).
[6] See `http://www.bethe-salpeter.org`.
[7] S. Ismail-Beigi, Phys. Rev. B **73**, 233103 (2006).
[8] R. Hambach, Ph.D. thesis, Ecole Polytechnique, Palaiseau (France) (2010).
[9] L. Sponza, Ph.D. thesis, Ecole Polytechnique, Palaiseau (France) (2013).
[10] M. S. Hybertsen and S. G. Louie, Phys. Rev. B **34**, 5390 (1986).
[11] P. Cudazzo, M. Gatti, and A. Rubio, Phys. Rev. B **86**, 195307 (2012).
[12] P. Cudazzo, M. Gatti, A. Rubio, and F. Sottile, Phys. Rev. B **88**, 195152 (2013).
[13] P. Cudazzo, F. Sottile, A. Rubio, and M. Gatti, Journal of Physics: Condensed Matter **27**, 113204 (2015).
[14] W. Hanke and L. J. Sham, Phys. Rev. Lett. **43**, 387 (1979).
[15] M. Rohlfing and S. G. Louie, Phys. Rev. B **62**, 4927 (2000).
[16] F. Bassani and G. P. Parravicini, *Electronic States and Optical Transitions in Solids* (Pergamon Press, 1975).
[17] G. H. Wannier, Phys. Rev. **52**, 191 (1937).
[18] R. S. Knox, *Theory of Excitons* (Academic Press, 1963).
[19] G. Dresselhaus, Journal of Physics and Chemistry of Solids **1**, 14 (1956).
[20] M. Altarelli and N. O. Lipari, Phys. Rev. B **15**, 4898 (1977).
[21] A. Molina-Sánchez, D. Sangalli, K. Hummer, A. Marini, and L. Wirtz, Phys. Rev. B **88**, 045412 (2013).
[22] D. Y. Qiu, F. H. da Jornada, and S. G. Louie, Phys. Rev. Lett. **111**, 216805 (2013).
[23] M. M. Ugeda, A. J. Bradley, S.-F. Shi, F. H. da Jornada, Y. Zhang, D. Y. Qiu, W. Ruan, S.-K. Mo, Z. Hussain, Z.-X. Shen, F. Wang, S. G. Louie, and M. F. Crommie, Nat Mater **13**, 1091 (2014).
[24] Z. Ye, T. Cao, K. O/'Brien, H. Zhu, X. Yin, Y. Wang, S. G. Louie, and X. Zhang, Nature **513**, 214 (2014).
[25] X. Wang, A. M. Jones, K. L. Seyler, V. Tran, Y. Jia,

H. Zhao, H. Wang, L. Yang, X. Xu, and F. Xia, Nat Nano **10**, 517 (2015).
[26] V. Tran, R. Soklaski, Y. Liang, and L. Yang, Phys. Rev. B **89**, 235319 (2014).
[27] O. Pulci, P. Gori, M. Marsili, V. Garbuio, R. D. Sole, and F. Bechstedt, EPL (Europhysics Letters) **98**, 37004 (2012).
[28] W. Wei and T. Jacob, Phys. Rev. B **87**, 115431 (2013).
[29] W. Wei and T. Jacob, Phys. Rev. B **88**, 045203 (2013).
[30] H. Liu, A. T. Neal, Z. Zhu, Z. Luo, X. Xu, D. Tomnek, and P. D. Ye, ACS Nano **8**, 4033 (2014), pMID: 24655084, http://dx.doi.org/10.1021/nn501226z.
[31] J. Qiao, X. Kong, Z.-X. Hu, F. Yang, and W. Ji, Nat Commun **5**, (2014).
[32] Y. Cai, G. Zhang, and Y.-W. Zhang, Scientific Reports **4**, 6677 (2014).